LUND UNIVERSITY

Remote sensing of vegetation dynamics in drylands

Evaluating vegetation optical depth (VOD) using AVHRR NDVI and in situ green biomass data over West African Sahel

Tian, Feng; Brandt, Martin; Liu, Yi Y.; Verger, Aleixandre; Tagesson, Torbern; Diouf, Abdoul A.; Rasmussen, Kjeld; Mbow, Cheikh; Wang, Yunjia; Fensholt, Rasmus

Remote sensing of vegetation dynamics in drylands: Evaluating vegetation optical depth (VOD) using AVHRR NDVI and *in situ* green biomass data over West African Sahel

Feng Tian [a,b,*], Martin Brandt [a], Yi Y. Liu [c], Aleixandre Verger [d], Torbern Tagesson [a], Abdoul A. Diouf [e], Kjeld Rasmussen [a], Cheikh Mbow [f], Yunjia Wang [b], Rasmus Fensholt [a]

[a] Department of Geosciences and Natural Resource Management, University of Copenhagen, 1350 Copenhagen, Denmark
[b] School of Environment Science and Spatial Informatics, China University of Mining and Technology, 221116 Xuzhou, China
[c] ARC Centre of Excellence for Climate Systems Science & Climate Change Research Centre, University of New South Wales, Sydney 2052, Australia
[d] CREAF, Cerdanyola del Vallès, 08193, Catalonia, Spain
[e] Centre de Suivi Ecologique (CSE), BP, 15532 Dakar-Fann, Senegal
[f] Science Domain 6, ICRAF (World Agroforestry Center), 00100, Nairobi, Kenya

ARTICLE INFO

ABSTRACT

Monitoring long-term biomass dynamics in drylands is of great importance for many environmental applications including land degradation and global carbon cycle modeling. Biomass has extensively been estimated based on the normalized difference vegetation index (NDVI) as a measure of the vegetation greenness. The vegetation optical depth (VOD) derived from satellite passive microwave observations is mainly sensitive to the water content in total aboveground vegetation layer. VOD therefore provides a complementary data source to NDVI for monitoring biomass dynamics in drylands, yet further evaluations based on ground measurements are needed for an improved understanding of the potential advantages. In this study, we assess the capability of a long-term VOD dataset (1992–2011) to capture the temporal and spatial variability of *in situ* measured green biomass (herbaceous mass and woody plant foliage mass) in the semi-arid Senegalese Sahel. Results show that the magnitude and peak time of VOD are sensitive to the woody plant foliage whereas NDVI seasonality is primarily governed by the green herbaceous vegetation stratum in the study area. Moreover, VOD is found to be more robust against typical NDVI drawbacks of saturation effect and dependence on plant structure (herbaceous and woody compositions) across the study area when used as a proxy for vegetation productivity. Finally, both VOD and NDVI well reflect the spatial and inter-annual dynamics of the *in situ* green biomass data; however, the seasonal metrics showing the highest degree of explained variance differ between the two data sources. While the observations in October (period of *in situ* data collection) perform best for VOD ($r^2 = 0.88$), the small growing season integral (sensitive to recurrent vegetation) have the highest correlations for NDVI ($r^2 = 0.90$). Overall, in spite of the coarse resolution, the study shows that VOD is an efficient proxy for estimating green biomass of the entire vegetation stratum in the semi-arid Sahel and likely also in other dryland areas.

© 2016 Elsevier Inc. All rights reserved.

1. Introduction

Improved understanding of changes in dryland biomass, including above ground vegetation mass of both the green component (herbaceous and woody plant foliage) and non-green woody component (woody stems and branches), is relevant to the understanding of the global carbon balance given that approximately 41% of the Earth's terrestrial surface is covered by drylands (Adeel et al., 2005). Recent studies showed that dryland biomass is a more dominant driver of global carbon cycle inter-annual variability as compared to the tropical rainforests (Ahlstrom et al., 2015; Poulter et al., 2014). An improved understanding of spatiotemporal trends in dryland biomass has become the subject of increased interest due to the impacts of current global changes and concern for the sustainability of human livelihoods.

Optical remote sensing provides a unique way of achieving full coverage of global drylands and has facilitated monitoring of biomass dynamics since the early 1980s, using the normalized difference vegetation index (NDVI) derived from reflectance of the red and near-infrared bands of a wide array of instruments, including the NOAA (National Oceanic and Atmospheric Administration) AVHRR (Advanced Very High Resolution Radiometer) which provides the longest record. As a measurement of chlorophyll abundance and energy absorption (Myneni & Hall, 1995; Tucker & Sellers, 1986), NDVI has been widely used as a proxy for the vegetation productivity (*e.g.* Myneni, Keeling,

Tucker, Asrar, and Nemani (1997) and Nemani et al. (2003)). However, several well-known limitations of NDVI for robust estimation of biomass in drylands exist. NDVI is sensitive to the green components and insensitive to woody components where the majority of carbon is stored (Tucker, 1979). Also, above ground vegetation production is not always linked to greenness in a uniform way and the plant structure (herbaceous and woody compositions) and vegetation species composition have been shown to impact the biomass-NDVI relationship (Goetz, Prince, Goward, Thawley, & Small, 1999; Mbow, Fensholt, Rasmussen, & Diop, 2013; Prince & Goward, 1995; Wessels et al., 2006) as well as soil color and moisture content (Huete, 1988). Moreover, atmospheric effects (e.g. water vapor, clouds and aerosols) contaminate images retrieved from the red and near-infrared bands in general and from the spectrally wide AVHRR bands in particular (Holben, 1986). This is not only inherent to tropical moist regions but also a problem in semi-arid areas like the African Sahel characterized by a distinctive growing season, which prevailing cloud cover often obscures regular monitoring of vegetation resources (Fensholt et al., 2007; Fensholt et al., 2011). Also, optical remote sensing during the dry season can be strongly influenced by atmospheric dust (e.g. the cold-dry and dusty trade wind known as the Harmattan) causing a noisy NDVI signal (Achard & Blasco, 1990; Ahearn & de Rooy, 1996). Finally, a well-known factor reducing the capability of NDVI to estimate biomass is the saturation effect due to the strong absorption in the red wavelength (Sellers, 1985). With an increasing amount of green vegetation, the sensitivity of NDVI is reduced and surface (or bottom of atmosphere, BOA) reflectance reaches a saturation point dependent on the specific response function of the satellite sensor (Gitelson, Kaufman, & Merzlyak, 1996). Despite the lower amount of green vegetation present in dryland areas, NDVI saturation effects have also been reported to impact vegetation monitoring (Fensholt, 2004; Milich & Weiss, 2000; Olsson, Eklundh, & Ardö, 2005).

Several previous studies have investigated vegetation dynamics based on satellite passive microwave observations (Becker & Choudhury, 1988; Choudhury, Tucker, Golus, & Newcomb, 1987; Jones, Jones, Kimball, & McDonald, 2011; Konings et al., 2016; Min & Lin, 2006; Njoku & Chan, 2006; Cui, Shi, Du, Zhao, & Xiong, 2015; Shi et al., 2008). Unlike the optical remote sensing based vegetation indexes (sensitive to greenness, i.e. chlorophyll concentrations), the vegetation information retrieved from satellite passive microwave observations (here referred as vegetation optical depth, VOD) is sensitive to the water content in the total aboveground vegetation, including both green (e.g. herbaceous and woody plant foliage) and non-green (e.g. woody stems and branches) components (Shi et al., 2008). For a given area of canopy cover, herbaceous and woody plant foliage may show similar greenness level (measured by reflectance) whereas being characterized by different levels of water content due to the different plant structures. Also, the temporal variation in water content of herbaceous and woody vegetation would be distinctly different dependent on the specific vegetation species and therefore VOD is expected to provide complementary information on biomass variability to NDVI (Jones, Kimball, & Jones, 2013). Furthermore, due to the longer wavelength and stronger penetration capacity of microwave, VOD is insensitive to atmosphere and cloud contamination effects and can therefore provide valid global observations at almost daily frequency, of benefit to land surface phenology monitoring (Guan et al., 2014; Jones, Kimball, Jones, & McDonald, 2012). Finally, VOD is reported to be less prone to saturation effect than NDVI (Jones et al., 2011). These features all together make VOD a promising coarse spatial resolution (>10 km) proxy for biomass assessment at regional to global scales, despite low accuracy of VOD retrievals for pixels with open water bodies (Jones et al., 2011).

Recently, a long-term VOD dataset covering more than 20 years was generated by combining observations from a series of passive microwave instruments (Liu, de Jeu, McCabe, Evans, & van Dijk, 2011a; Liu et al., 2015). This unique dataset provides new opportunities for gaining insights of global vegetation changes from the microwave region of the

spectrum over a period almost comparable with AVHRR sensors. Based on this VOD dataset, long-term changes in global drylands have been investigated and, as expected, it is found that the inter-annual variations of VOD are mainly driven by precipitation (Andela, Liu, van Dijk, de Jeu, & McVicar, 2013; Liu, van Dijk, McCabe, Evans, & de Jeu, 2013b; Liu et al., 2013a). However, to the authors' best knowledge no analysis including in situ biomass measurements has been conducted to examine and evaluate the spatial and temporal dynamics of VOD data in relation to different compositions of annual herbaceous and perennial woody vegetation. Moreover, the annual sum/maximum and the growing season integral of NDVI have a proven record of showing realistic estimations for biomass in drylands (Diouf et al., 2015; Meroni et al., 2014; Prince, 1991; Tucker, Vanpraet, Boerwinkel, & Gaston, 1983; Wessels et al., 2006). However, whether these seasonal metrics should be applied in the same way for VOD data has not yet been analyzed.

The overall objective of this study is to gain an improved understanding of the performance of VOD data for monitoring long-term vegetation dynamics in dryland areas. This is achieved by comparing with the well-known NDVI based approach and in situ measurements of green biomass (herbaceous mass and woody plant foliage mass) in the semi-arid Senegalese Sahel during the period 1992–2011. Firstly, we explore the VOD responses to different herbaceous and woody compositions in the study area characterized by a pronounced north–south gradient in woody cover and green biomass. Then, we analyze the capability of different VOD metrics to assess green biomass dynamics in both spatial and temporal domains.

2. Data

2.1. Study area

All in situ sites are located in the semi-arid Sahel zone of Senegal (Fig. 1). The Sahel can be separated into three zones, following a rainfall gradient from the northern Sahel (150–300 mm annual rainfall), over the central Sahel (300–500 mm) to the southern Sahel (500–700 mm) (Brandt et al., 2016). Driven by the rainfall, the vegetation density also shows a clear north–south increasing gradient with mean annual green biomass varying from approximately 1000 kg DM (dry matter) ha^{-1} at the northern sites to >4500 kg DM ha^{-1} at the southern sites (calculated from data described in Section 2.4). The entire region is characterized by savannas consisting of herbaceous and woody trees and shrubs. The herbaceous stratum is dominated by annual plants growing from late June to early October, however strongly dependent on annual rainfall distribution (Huber, Fensholt, & Rasmussen, 2011). The phenological behavior of woody plants is evergreen, semi-evergreen or deciduous (Le Houérou, 1980), showing distinct different phenological cycles as compared to the herbaceous stratum present only during the rainy season. A mean woody cover map (2000–2013) produced by Brandt et al. (2016) at 1 km spatial resolution was used here to indicate the spatial variation of plant structure in the study area, with a woody cover increase from <3% in the north to >40% in the south. Whereas herbaceous vegetation dominates the green biomass in the north, the woody plant foliage produces higher biomass than the herbaceous stratum in the south (Diouf et al., 2015).

2.2. VOD data

The VOD is a function of the vegetation dielectric properties, responding primarily to the water content in total aboveground vegetation including green and non-green components, varying with the plant structure as well as the sensor wavelength and viewing angle (Jackson & Schmugge, 1991). Briefly, the satellite based passive microwave observations (brightness temperature, T_b) consist of three components: 1) the radiation from the soil layer attenuated by the overlaying vegetation, 2) the upward radiation from the vegetation, and 3) the downward radiation from the vegetation, reflected upward by the soil layer and
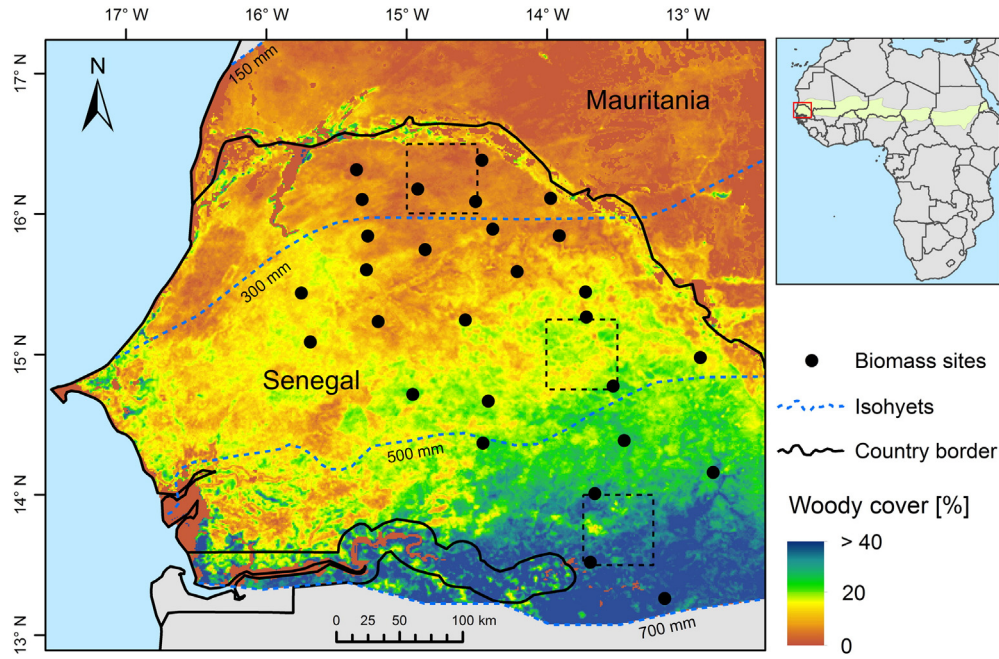
Fig. 1. Location of *in situ* observation sites in Senegal with a background showing mean woody cover during 2000–2013 (Brandt et al., 2016). The areas indicated by the dashed black boxes are further analyzed in Fig. 4A. The Sahel region and the Senegalese study area are highlighted in the map of Africa (top right).

again attenuated by the vegetation (Mo, Choudhury, Schmugge, Wang, & Jackson, 1982) as shown in the Eq. (1).

$$T_b^P = T_{S_{er}}^P \Gamma^P + (1-\omega^P)T_C(1-\Gamma^P) + (1-e_r^P)(1-\omega^P)T_C(1-\Gamma^P)\Gamma^P \quad (1)$$

where P is the polarization (horizontal and vertical); T_S and T_C are the thermometric temperatures of the soil and the canopy, respectively; e_r is the soil emissivity determined by soil moisture, temperature and roughness; Ω is the single scattering albedo; Γ is the vegetation transmissivity determined by VOD (τ, dimensionless) and observing incidence angle (μ) in the Eq. (2).

$$\Gamma = exp(-\tau/cos\mu). \quad (2)$$

The Land Parameter Retrieval Model (LPRM) retrieval algorithm (Meesters, de Jeu, & Owe, 2005; Owe, de Jeu, & Holmes, 2008; Owe, de Jeu, & Walker, 2001), developed from the above radiative transfer model, can derive soil moisture and VOD simultaneously under the assumptions of a constant single scattering albedo, canopy surface temperature equal to soil surface temperature during night time, equality of vegetation parameters for both horizontal and vertical polarizations, and a fixed surface roughness value.

LPRM can be applied to observations from different satellites with varying microwave wavelengths and viewing angles. Accordingly, VOD datasets were derived from observations of a series of passive microwave instruments onboard different satellites, including the Special Sensor Microwave Imager (SSM/I) of the Defense Meteorological Satellite Program, the Advanced Microwave Scanning Radiometer — Earth Observing System (AMSR-E) onboard the Aqua satellite, and the radiometer of the WindSat (Liu et al., 2015). The lowest microwave frequency of each sensor of SSM/I (19.4 GHz), AMSR-E (6.9 GHz) and WindSat (6.8 GHz) were used. Due to the dependence of sensor characteristics, VOD values vary between these three instruments. However, these three sensors have reasonably long overlapping periods, and their temporal dynamics are highly correlated for most of the Earth's land surface and in drylands in particular. The cumulative distribution function (CDF) matching approach was therefore conducted to merge these three VOD datasets into one long term time series over 1992–2011 without influencing the inter-annual variations and long-term

changes of the original retrievals (Liu et al., 2011a; Liu et al., 2011b; Liu et al., 2012). In the merged VOD dataset, SSM/I observation is used from January 1992 through June 2002 before the AMSR-E started operating, while AMSR-E is used from July 2002 through September 2011. WindSat observation is used after AMSR-E stopped collecting data in early October 2011. The temporal consistency of this merged dataset was examined using both global and humidity zone averaged VOD anomaly series (similar to the method applied by Tian et al. (2015)) and found no artifacts in the time series to coincide with sensor shifts (see Supplementary material Fig. S1). The VOD value ranges from 0 to roughly 1.3 in the merged VOD dataset, and it is aggregated to 0.25 degree (~25 km) spatial resolution and monthly intervals.
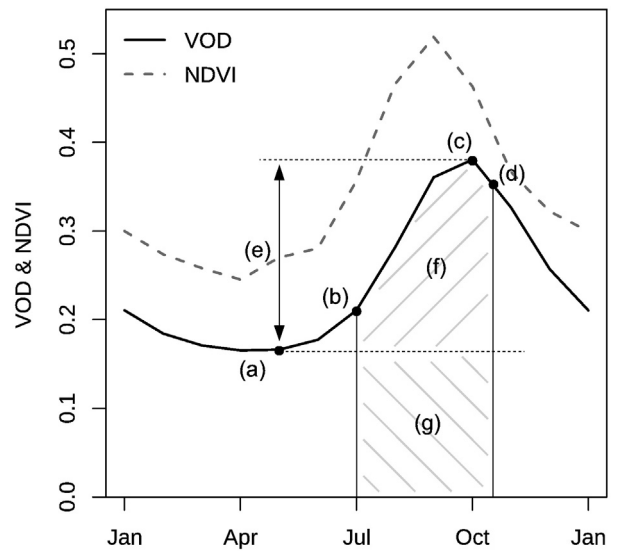
Fig. 2. Illustration of the seasonal vegetation metrics used in this study: (a) annual minimum, (b) start of season, (c) annual maximum, (d) end of season, (e) amplitude, (f) small integral, and (f) + (g) large integral. The VOD and NDVI curves are the mean of the entire study area (as shown in Fig. 1) during 1992–2011.

2.3. GIMMS3g AVHRR NDVI

Although the GIMMS (Global Inventory Modeling and Mapping Studies) NDVI product is not without problems (Horion, Fensholt, Tagesson, & Ehammer, 2014; Tian et al., 2015), it has been reported to be the most suitable for long-term vegetation analysis amongst several available long-term AVHRR NDVI datasets (Beck et al., 2011; Tian et al., 2015) and trend analysis of the GIMMS NDVI products have been shown to be in agreement with trends from MODIS (Moderate Resolution Imaging Spectroradiometer) NDVI products particularly in drylands (Dardel et al., 2014; Fensholt & Proud, 2012; Fensholt, Rasmussen, Nielsen, & Mbow, 2009). The latest version of the GIMMS AVHRR
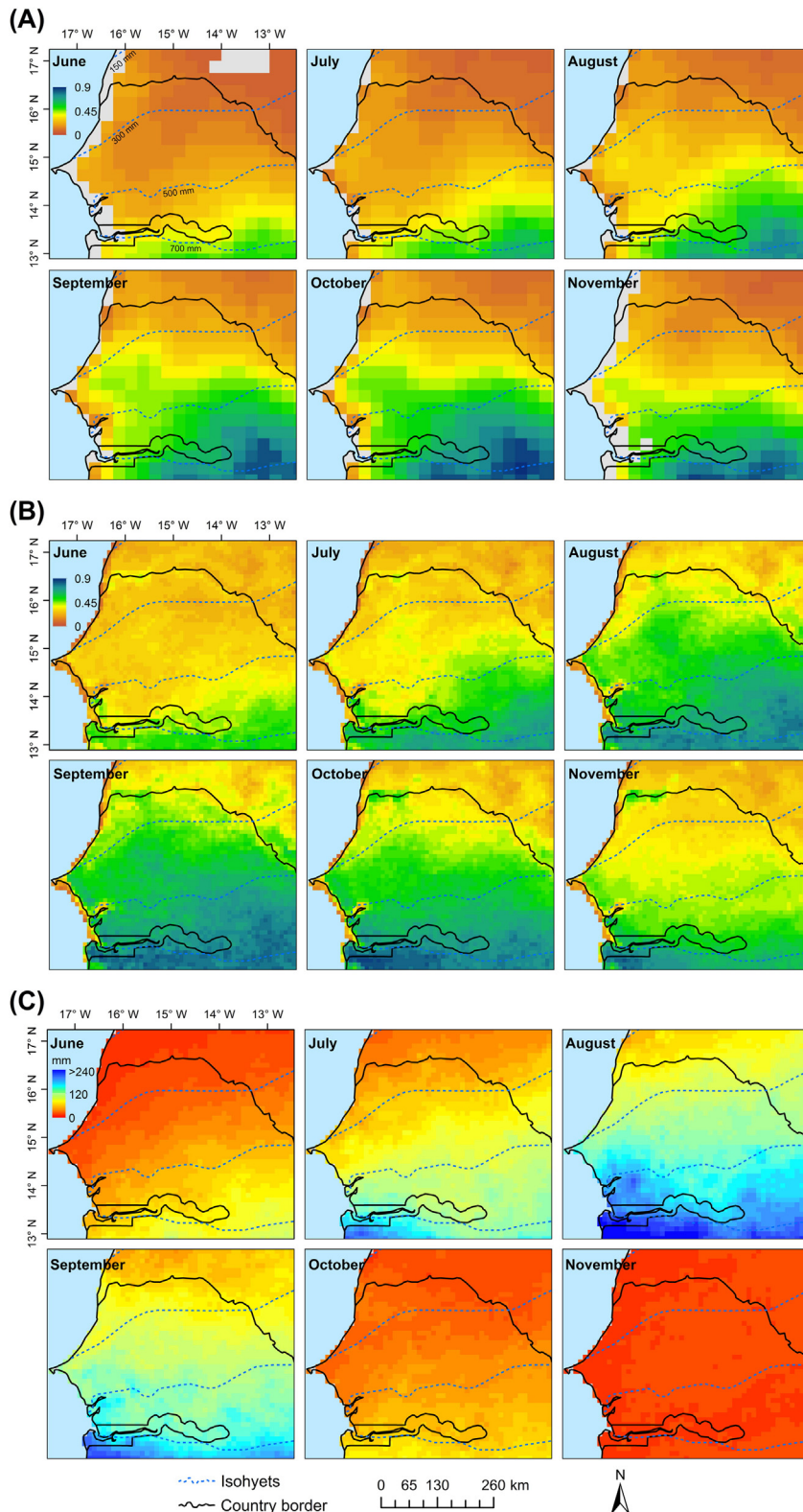

Fig. 3. Spatial patterns of monthly mean VOD (A), NDVI (B) and annual rainfall (C) during 1992–2011 from June to November.

NDVI data (GIMMS3g) was therefore used in this study and includes the following overall pre-processing steps (for a detailed description refer to Pinzon and Tucker (2014)): The AVHRR channel 1 (visible band) and channel 2 (near-infrared band) are calibrated by applying time-varying vicarious calibrations methods (Cao, Xiong, Wu, & Wu, 2008; Los, 1998; Vermote & Kaufman, 1995; Wu, Sullivan, & Heidinger, 2010). The varying solar zenith angle effects on NDVI values (caused by orbital drift) are reduced using an adaptive empirical mode decomposition/reconstruction procedure (Pinzon, Brown, & Tucker, 2005). The AVHRR/2 and AVHRR/3 NDVI probability density functions were calibrated by applying a Bayesian analysis using the SeaWiFS (Sea-Viewing Wide Field-of-view Sensor) NDVI data as prior information (Pinzon & Tucker, 2014). Maximum value compositing over 15 days was applied to reduce the atmospheric effects. Furthermore, strato-spheric aerosol correction was applied during the El Chichon (April 1982–December 1984) and Mt. Pinatubo (June 1991–December 1993) volcanic stratospheric aerosol periods (Tucker et al., 2005). The GIMMS3g NDVI dataset provides bi-weekly images subsampling within spatial windows of 1/12°. We averaged the bi-weekly NDVI values into monthly observations during 1992–2011 for consistency with the VOD dataset whereas the original spatial resolution of GIMMS3g NDVI was kept.

2.4. In situ measurements

Annual biomass data was collected by the Centre de Suivi Ecologique (CSE) in Senegal from 1992 to 2011 (except for 2004). The measurements were conducted at the end of the growing season (October) and the data has shown to be consistent with satellite time series (Brandt et al., 2015). Biomass of herbaceous and woody plant foliage layers were assessed separately and summed to obtain the green biomass in kg DM ha^{-1}.

The herbaceous collection followed the original method proposed by the International Livestock Centre for Africa (ILCA) (Diouf, Sall, Wélé, & Dramé, 1998) based on stratification of the herbaceous layer into four strata (bare soil patches and low, medium and high herbaceous bulk density). At each field site, a 1 km transect was selected, along which 35 to 100 one square meter plots were randomly placed, considering the vegetation stratification. For each of the strata, all fresh vegetation collected was weighed and three 200 g samples of each stratum were dried in an oven to obtain the dry matter to wet weight ratio. The dry matter weight of each stratum is obtained by multiplying the mean wet weight by the dry matter ratio. Then, the site herbaceous mass is calculated by weighting the mean mass of each stratum by the relative frequency of the stratum along the transect.

Foliage biomass measurements of trees and shrubs were performed for each site in two steps: 1) every two years, all species were sampled within four circular plots (of 1/16 to 1 ha) placed every 200 m along the selected transect. Along with other parameters, the circumferences of alive trunks were measured for calculation of the potential woody foliage biomass using the allometric relationships established for Sahelian tree and shrub species (Cissé, 1980; Diallo, Diouf, Hanan, Ndiaye, & PrÉVost, 1991; Diouf & Lambin, 2001; Hiernaux, 1980). 2) These potential values were then adjusted to each particular year and site conditions with leaf samples of 10 branchlets from each of the most representative species. Then, the total woody foliage biomass of each site was obtained by summing up all woody species analyzed. A detailed description of the method is provided by Diouf et al. (2015).

We examined the VOD pixels covering each site with Google Earth and excluded 5 highly heterogeneous plots that are located either close to rivers or mixed cropping and forest areas (whereas the measurements were taken in the forest area only), leaving 27 relatively homogeneous sites (Fig. 1) with 334 measurements for further analysis (not all sites were surveyed by CSE each year).

2.5. Rainfall data

The ARC2 (African Rainfall Climatology version 2) daily rainfall data (0.1° spatial resolution) (Novella & Thiaw, 2013) were used in the study. For temporal consistency with the VOD dataset, we summed the daily rainfall values into monthly observations during 1992–2011, whereas the original spatial resolution of the ARC2 data was kept.

3. Methods

3.1. Exploring VOD responses to herbaceous and woody composition

To understand the VOD responses to herbaceous and woody compositions, we compared VOD spatial patterns and seasonal variations to NDVI over the study area (characterized by a clear north–south vegetation gradient). The pixel-wise monthly VOD, NDVI and ARC2 rainfall means across the entire period (1992–2011) were calculated for the study area and to better illustrate the differences between VOD and NDVI we further examined the seasonal patterns of three sub regions (Fig. 1) along the north–south gradient (with mean woody cover of 4%, 16% and 32%, respectively). The VOD and NDVI seasonal variations were interpreted with the typical phenological behaviors (i.e. the temporal distribution of green biomass) of herbaceous and dominant woody species in the study area (evergreen, semi-evergreen and decid-uous), produced by Mougin, Lo Seena, Rambal, Gaston, and Hiernaux (1995); Mougin et al. (2014) and Brandt et al. (2016) who used the STEP (Sahelian transpiration, evaporation, and productivity) model (Mougin et al., 1995) with ground measurements as input data. Moreover, the in situ herbaceous and woody plant foliage biomass data were plotted against the corresponding annual maximum VOD/NDVI, respectively. Finally, we compared the relationships between annual maximum VOD/NDVI (calculated from the long-term monthly mean during 1992–2011) and woody cover over the study area. In this context, the woody cover data was averaged to the VOD spatial resolution while the median of NDVI pixels overlapping the VOD pixel was used.

3.2. Evaluating VOD and NDVI metrics for assessing green biomass dynamics

3.2.1. Seasonal metrics

The annual maximum, annual sum, growing season large integral (integration of absolute values during the growing season) and small integral (integration of amplitudes during the growing season) (Fig. 2) have been widely used to estimate dryland biomass with NDVI time series observations based on linear regression (de Jong, de Bruin, de Wit, Schaepman, & Dent, 2011; Fensholt et al., 2015; Tian et al., 2013). Here, we tested the performance of these metrics for VOD data against the annual in situ green biomass data at 27 sites over 20 years using ordinary least square linear regressions. As the in situ green biomass data were collected during month of October, we also examined the performance of VOD October observations. For comparison purposes, NDVI data was also analyzed against the in situ green biomass data. The growing season integrals were calculated using the TIMESAT software (Jonsson & Eklundh, 2002, 2004). The start of season was set to 20% of the amplitude for both VOD and NDVI data. To try and be in line with the average time of in situ data collection, the end of season was set to 80% of the amplitude for the VOD data and 50% for the NDVI data (different thresholds applied due to the later drop of VOD values as compared to NDVI as shown in Fig. 2).

3.2.2. Data comparison

The comparisons between VOD/NDVI metrics and in situ green biomass data were performed in two steps. (1) We assessed the performance of VOD and NDVI metrics for assessing green biomass dynamics at the pixel level across a gradient of increasing biomass from north to south. For each year during 1992–2011, we calculated
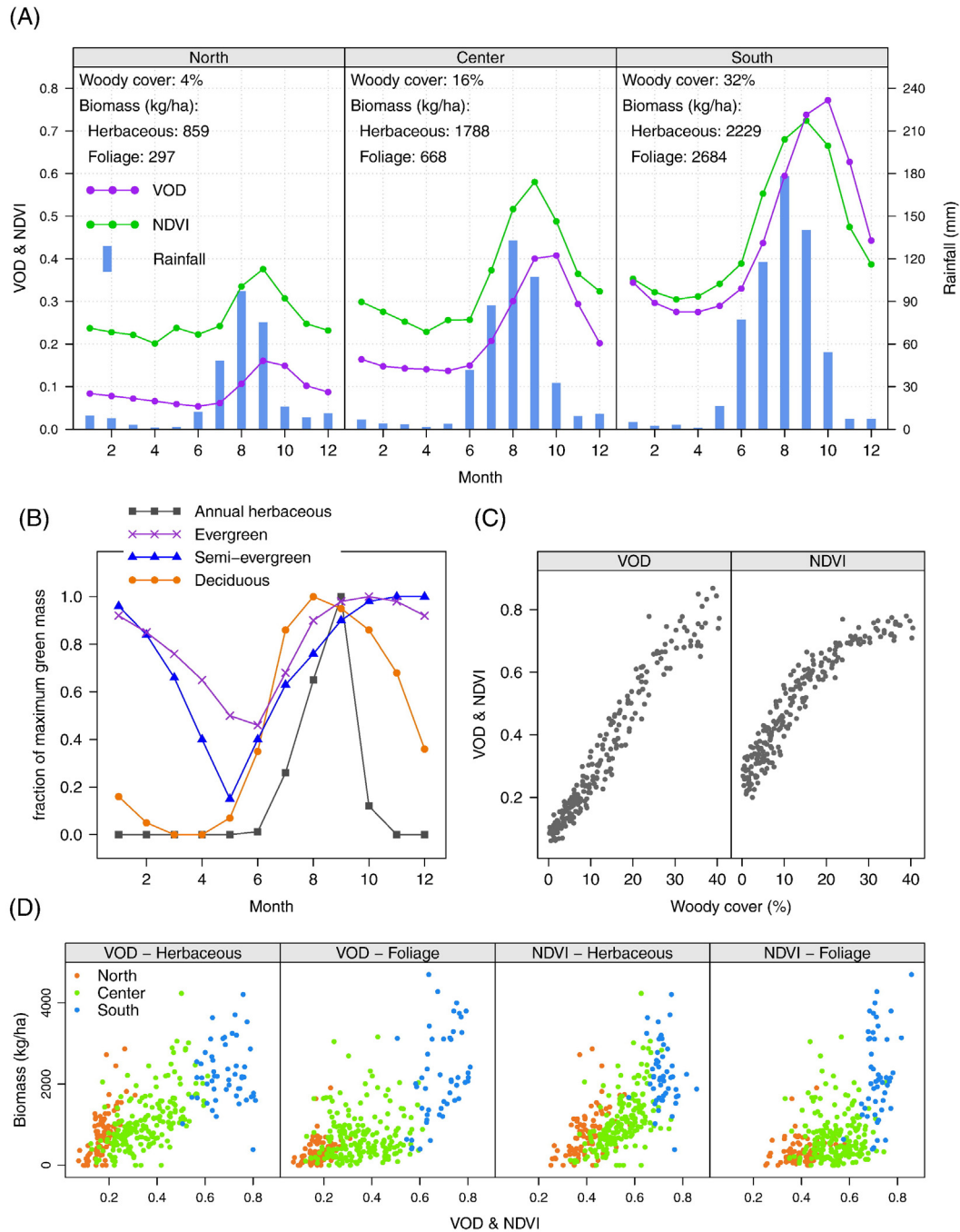
Fig. 4. (A) Seasonal patterns of monthly mean VOD, NDVI and rainfall during 1992–2011 in the sub regions of northern, central and southern parts of the study area (average of all pixels in each of the dashed black boxes in Fig. 1). The biomass of herbaceous and woody plant foliage is given by averaging the *in situ* sites within each selected area. (B) Phenology of typical Sahelian herbaceous and woody vegetation (expressed as fraction of maximum green mass, extracted from Mougin et al. (1995); Mougin et al. (2014) and Brandt et al. (2016)). Although variations can be observed from north to south, the general phenological behavior follows these curves. (C) Spatial relationships of woody cover and the annual maximum VOD/NDVI calculated from the monthly mean during 1992–2011 over the study area. (D) Comparisons between *in situ* herbaceous and woody plant foliage biomass data and the corresponding annual maximum VOD/NDVI values.

all the VOD and NDVI seasonal metrics for each pixel overlapping the *in situ* sites. Then, each of the seasonal metric was regressed against the corresponding biomass data for the sites located in the northern, central, southern and entire study area, respectively. (2) We focused on the capabilities of VOD and NDVI metrics for assessing green biomass inter-annual dynamics over all *in situ* sites. Due to differences in the spatial resolution (VOD 25 km, NDVI 8 km, and biomass data 1 km), the heterogeneity effect inevitably introduces bias between *in situ* measurements and remote sensing observations, impeding a successful evaluation of the temporal dynamics of the VOD and

NDVI data. To reduce this bias while preserving the aspects of temporal dynamics, we therefore averaged all the available *in situ* data over the entire study area for each year and the corresponding pixel-scale VOD/NDVI metrics calculated in the first step, respectively. This averaging method has been widely applied for evaluating satellite observations using *in situ* measurements (Dardel et al., 2014; Jackson et al., 2010; Tagesson et al., 2013; Zeng et al., 2015). The coefficient of determination (r^2) of Pearson product–moment correlation and root mean square error (RMSE) were calculated for each pair of comparison in both steps.

4. Results

4.1. VOD responses to herbaceous and woody compositions

The spatial patterns of VOD, NDVI and rainfall in the study area are shown for the months covering the rainy season (June–November) (Fig. 3). Despite the coarse spatial resolution of the VOD data, a clear north–south gradient is observed in a similar way to the spatial patterns of NDVI. The seasonal patterns of the selected sub regions (dashed black boxes in Fig. 1) are shown in Fig. 4A. VOD starts to increase simultaneously with NDVI for all sub regions in the study area, in line with the onset of the rainfall. During the growth phase, NDVI shows identical temporal development from north to south, reaching the second highest value in August, peaking in September and then decreasing in October to a lower level followed by a further drop in November. VOD data however, show high values in both September and October from north to south, with peak time changing from September in the north to October in the south. This shift in the VOD peak time is in line with the higher proportion of woody plant foliage (see the herbaceous and foliage biomass of each sub region in Fig. 4A) which is characterized by longer growing seasons and later peak time than the herbaceous stratum (Fig. 4B). Both herbaceous and woody plant foliage biomass exhibit an increasing gradient from north to south. The gradient of herbaceous biomass is well reflected by both annual maximum VOD and NDVI data, whereas VOD captures the gradient of foliage biomass better than NDVI which shows clearer saturation effect in the south (Fig. 4D). The higher sensitivity of VOD than NDVI to woody vegetation is also indicated by their respective relationships with woody cover (Fig. 4C). VOD increases linearly with increasing woody cover, whereas NDVI saturates around 25% of woody cover. Another noticeable point when comparing VOD/NDVI against woody cover is that the VOD values show less variation than NDVI values in areas of limited woody cover.

4.2. Performance of VOD and NDVI metrics for assessing green biomass dynamics

The scatter plots between pixel-scale VOD/NDVI metrics and plot-scale *in situ* green biomass data are shown in Fig. 5 and the r^2 and RMSE values for individual regions are summarized in Table 1. The statistical results for the averaged VOD/NDVI metrics and *in situ* green biomass data are summarized in Table 2 while Fig. 6 shows the performance of VOD and NDVI metrics, respectively, in relation to the temporal changes of *in situ* data. These results are interpreted in two complementary ways: (1) the performance of VOD and NDVI metrics across a gradient of increasing biomass, and (2) the performance of VOD and NDVI metrics for assessing inter-annual green biomass dynamics over all the *in situ* sites.

1) In line with the rainfall and woody cover, the green biomass is also characterized by an increasing gradient from north to south of the study area. Like the relationship with woody cover (Fig. 4C), the NDVI maximum shows clear saturation effect in the southern part while this is less pronounced for VOD maximum (Fig. 5). Taking all sites into account, all of the seasonal metrics show significant ($p < 0.01$) correlations with the green biomass data and the r^2 values (0.59–0.66 for VOD and 0.52–0.61 for NDVI) are higher as compared to those for individual parts of the study area (Fig. 5). With a large amount of observations in the central part (N = 191), significant correlations ($p < 0.01$) are obtained between biomass data and all seasonal metrics (r^2 equals 0.21–0.35 for VOD and 0.19–0.28 for NDVI) (Table 1). In the northern part (N = 91), the seasonal metrics (except for NDVI large integral with $p < 0.05$ and $r^2 = 0.07$) also show significant correlations ($p < 0.01$) with the *in situ* green biomass data and the r^2 values (0.27–0.42 for VOD and 0.20–0.33 for NDVI) are comparable to those in the central part. The seasonal metrics show poorer performance (lower r^2 values, 0.06–0.12 for VOD

and 0.05–0.21 for NDVI) in the southern part (N = 52), with several metrics showing insignificant correlations ($p > 0.05$ for VOD annual sum, small and large integrals and NDVI annual max and small integral) with the *in situ* green biomass data. The VOD metrics outperform the NDVI counterparts in the northern, central and entire parts of the study area (except for the small integral in the central part). In the southern part, NDVI metrics of October, annual sum and large integral show higher r^2 than the VOD counterparts although both data types perform poorly in this part.

2) By averaging all the sites to reduce the bias caused by scale differences between satellite and ground observation footprints, all the VOD/NDVI metrics show improved correlation with the *in situ* green biomass data (Table 2) as compared to the pixel versus plot scale comparisons (Fig. 5). The metrics derived from both VOD and NDVI are able to reproduce the averaged *in situ* green biomass
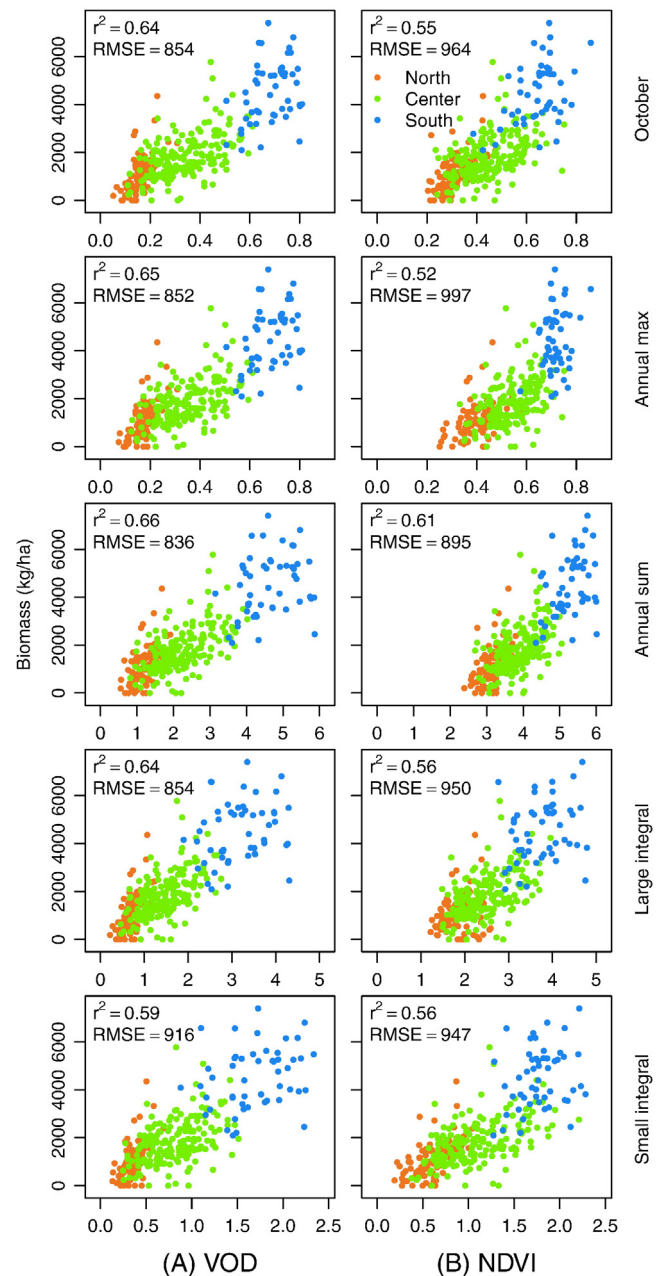

Fig. 5. Scatter plots between *in situ* green biomass data (herbaceous + foliage) collected at the end of growing season (October) and seasonal metrics ((A) VOD and (B) NDVI) of October, annual max, annual sum, large integral and small integral. The r^2 and RMSE are calculated from all the observations (N = 334) and are significant at 0.01 level.

Table 1

r^2 values between different VOD/NDVI metrics and *in situ* green biomass measurements of the sites located in the northern, central, southern part of the study area (corresponding to the scatter plots in Fig. 5). The number of observations is given as "N". Asterisks denote significant linear correlations at 0.01 "**" and 0.05 "*" levels, respectively.

Metrics	VOD						NDVI					
	North N = 91		Centre N = 191		South N = 52		North N = 91		Centre N = 191		South N = 52	
	r^2	RMSE	r^2	RMSE	r^2	RMSE	r^2	RMSE	r^2	RMSE	r^2	RMSE
October	0.38**	588	0.30**	755	0.12*	1177	0.31**	621	0.21**	805	0.21**	1121
Annual max	0.42**	568	0.30**	758	0.12*	1182	0.20**	671	0.19**	816	0.05	1229
Annual sum	0.27**	641	0.35**	728	0.07	1216	0.23**	656	0.23**	794	0.16**	1156
Large integral	0.37**	594	0.32**	745	0.06	1221	0.07*	723	0.26**	778	0.08*	1207
Small integral	0.33**	614	0.21**	806	0.06	1219	0.33**	613	0.28**	766	0.06	1217

inter-annual dynamics at a similar level (Table 2 and Fig. 6). However, the metrics characterized by the highest degree of explained variance differ between the two data sources. The VOD October shows the best performance ($r^2 = 0.88$) amongst all of the VOD metrics, closely followed by the annual sum ($r^2 = 0.87$), annual max ($r^2 = 0.86$) and then the large integral ($r^2 = 0.83$) whereas the VOD small integral shows poorest performance ($r^2 = 0.64$) amongst all VOD and NDVI metrics. On the contrary, the NDVI small integral shows the best performance ($r^2 = 0.90$) while October NDVI shows the poorest ($r^2 = 0.68$). The NDVI large integral ($r^2 = 0.82$) shows a better performance than the NDVI annual sum ($r^2 = 0.72$) and annual max ($r^2 = 0.70$).

5. Discussion

5.1. VOD dataset limitations

The accuracy of the LPRM VOD retrievals depends on the LPRM soil moisture retrievals which are in turn expected to be of varying accuracy over different regions due to the assumptions made in the LPRM algorithm. Gruhier et al. (2010) found that LPRM soil moisture retrievals agrees well with ground soil moisture measurements in Mali, both in terms of absolute values and temporal dynamics. These findings suggest reasonable confidence in the LPRM VOD retrievals over our study area in the West African Sahel. However, some studies showed that the LPRM soil moisture retrievals exhibits a wet bias compared with the ground soil moisture in the US and Tibet (Jackson et al., 2010; Leroux et al., 2014; Zeng et al., 2015). Hence, the VOD retrievals over these study areas should be used with caution. Yet, the reported wet biases are at similar level for the same time (*i.e.* same Julian day or same month) of different years. Therefore, it would be expected that the influence of wet biased soil moisture on the VOD retrievals is similar for the same time of different years, thereby having less influence on analyses of inter-annual variations and long-term changes as compared to studies of intra-annual seasonality in the VOD dataset. The long-term VOD dataset is generated from microwave observations of three different sensors i.e. SSM/I, AMSR-E and WinSat with the frequency of 19.4 GHz, 6.9 GHz and 6.8 GHz, respectively. The lower the microwave frequency, the stronger is the penetration capacity and consequently
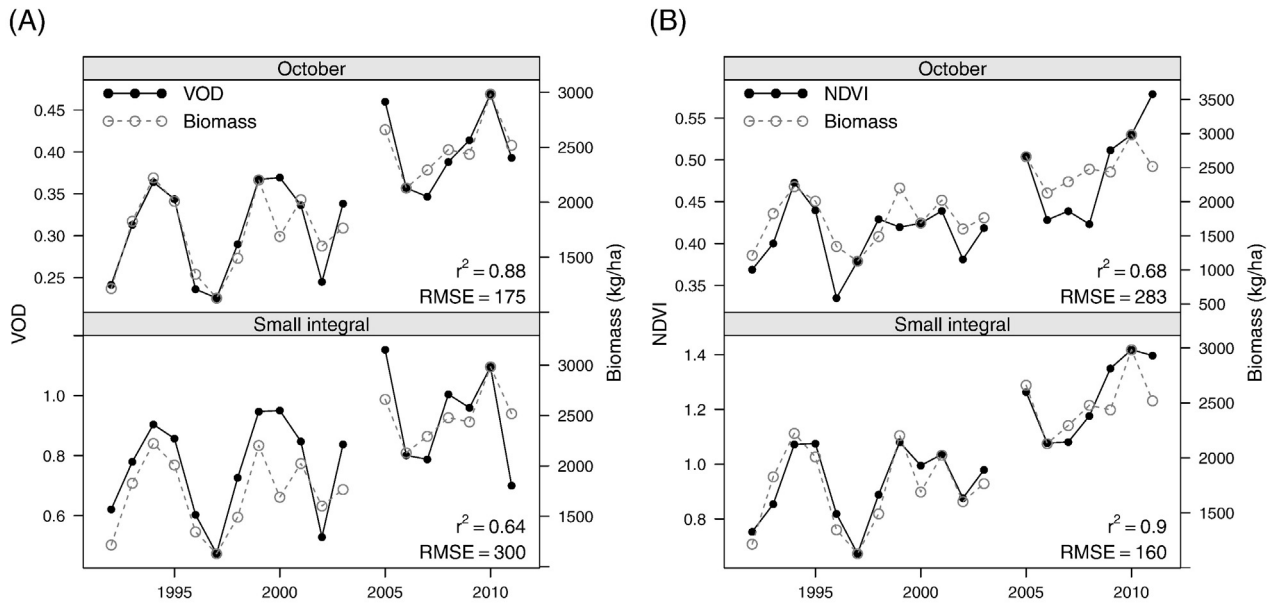
the more reliable are LPRM retrievals. Therefore, the uncertainty of the VOD retrievals from SSM/I is higher due to its higher microwave frequency. Ground-based measurements showed that the VOD is polarization dependent for agriculture fields with some expected preferential orientations (Wigneron, Chanzy, Calvet, & Bruguier, 1995). At satellite footprint scale, however, it may be reasonable to assume that the VOD is polarization independent as verified by Owe et al. (2001), especially for the randomly oriented crops and natural vegetation in the Sahel region. The current long-term VOD dataset is produced in a monthly temporal resolution which may not fully reflect the intra-seasonal vegetation dynamics in areas with highly dynamic vegetation like the Sahel.

5.2. VOD sensitivity to plant structure and species composition

VOD is sensitive to total water content but the coefficient of proportionality depends on the plant structure, as indicated by the larger scattering in the high woody cover values as compared to the low woody cover values (Fig 4C) and the different responses to herbaceous and woody plant foliage biomass data (Fig. 4D). However, the VOD sensitivity to plant structure is less than as for NDVI which shows clearer saturation effects when comparing with woody cover and woody plant foliage biomass data (Fig. 4C and D). Also, the VOD sensitivity to water content in woody stems varies with the canopy density. For dense rainforest areas, VOD reflects primarily the canopy water content varations (Jones, Kimball, & Nemani, 2014) whereas for savannas and woodlands (like our study area) the water content of the wood would also be captured by the VOD retrievals from low microwave frequency signals. Hence, the variation of water content of the wood would also contribute to the VOD seasonal patterns. However, water content of the wood is expected to be relatively stable over time (forms part of the VOD base level) as compared to the water content of herbaceous and foliage part (forms the VOD increment from the base level).

The *in situ* data collected at the Dahra field site (Supplementary material Fig. S2) shows that greenness and water content of the herbaceous stratum are highly linked particularly during the browning stage of the growing season, which is also likely to apply for the woody plant foliage. Therefore, by comparing the seasonal patterns of VOD and NDVI (Fig. 4A) with the intra-annual dynamics of green biomass (expressed as the fraction of maximum green mass in Fig. 4B), we can infer that the later peak time of the woody plant foliage (and likely the water content in the woody component) as compared to herbaceous vegetation result in the longer period of high VOD values (September and October) as compared to NDVI (peak in September). Consequently, VOD reflects the temporal development of woody vegetation better than NDVI, which was also concluded by Jones et al. (2013) for the application of monitoring forest recovery from wildfires.

Estimation of green biomass using the NDVI metrics has been reported to be influenced and hampered by varying herbaceous and woody compositions (Diouf et al., 2015; Wessels et al., 2006) and species composition (Mbow et al., 2013; Olsen, Miehe, Ceccato, & Fensholt, 2015) due to plant structure/species specific relationships

Table 2

Performance of different VOD and NDVI metrics for assessing *in situ* green biomass inter-annual dynamics (1992–2011). All the available sites over the study area for each year were averaged to reduce the bias caused by scale differences. All of the r^2 obtained are significant at the 0.01 level.

Metrics	VOD		NDVI	
	r^2	RMSE	r^2	RMSE
October	0.88	175	0.68	283
Annual max	0.86	186	0.70	274
Annual sum	0.87	178	0.72	263
Large integral	0.83	204	0.82	209
Small integral	0.64	300	0.90	160

Fig. 6. Comparisons of the inter-annual dynamics between mean of all the *in situ* green biomass data collected at the end of growing season (October) and the corresponding (A) VOD and (B) NDVI metrics characterized by the highest and lowest r². The ranges of y axis at both sides are adjusted to match the years with minimum and maximum *in situ* green biomass (1997 and 2010, respectively) in each sub plot for improved visualization.

between greenness and biomass. Our study shows that VOD may be a more robust proxy for the green biomass. This is supported by the generally higher correlations between VOD metrics and *in situ* green biomass data as compared to NDVI metrics (Fig.5 and Table 1), even though VOD pixels have coarser spatial resolution. Furthermore, in the northern part (dominated by herbaceous vegetation), the higher correlation between VOD and *in situ* green biomass data (Table 1) may indicate that VOD is more robust against herbaceous species composition variability. This is also supported by the less variation of the scatter plots (Fig. 4C) between VOD and low woody cover as compared to NDVI. However, this conclusion may be weakened by the larger influence of atmospheric effects and soil background on NDVI as compared to VOD.

5.3. Performance of seasonal metrics for VOD and NDVI

Averaging the VOD/NDVI metrics and *in situ* green biomass data over all the sites minimized the biases caused by scale differences between satellite and ground measurements, allowing for assessing the performance of different seasonal metrics (Table 2) with implications for the optimal use of VOD and NDVI for green biomass estimation. The good performance of VOD October observations (when ground measurements were collected) indicates that the water content in the total vegetation layer is highly correlated to the green biomass. The reason why the annual sum performs better than the large integral may be that the annual sum includes information on woody vegetation during the dry season (excluded in the large integral) which in turn contributes to the woody biomass foliage production in October. The relatively poorer performance of the VOD small integral is likely to be caused by the omission of the information on water content in woody component and the persistent part of the foliage (captured by the base level of the VOD curve) that plays an important role in the photosynthetic process for producing foliage mass. For NDVI, the best performance of the small integral in capturing biomass temporal dynamics was also documented for the Sahel by Fensholt et al. (2013) and Olsen et al. (2015). A possible reason could be that the annual herbaceous and woody plant foliage during growing season forms the dominant part of the net primary production (NPP) and that information on the green part of perennial vegetation (included in annual sum and large integral) is influenced by varying atmospheric conditions and soil background during the period

of the dry season (approximately 9 months). The artifacts of GIMMS3g NDVI product pronounced in Sahel dry season observations during 2004–2011 (Horion et al., 2014) also have greater impacts on the performance of the annual sum than the small integral. The NDVI annual max has been used as a proxy for the maximum vegetation productivity (Evans & Geerken, 2004; Fuller, 1998; Jeyaseelan, Roy, & Young, 2007). However, in a study by Olsson et al. (2005) a much more widespread greening of the Sahel was found when calculated from seasonal NDVI integrals as compared to trend estimates calculated from the seasonal NDVI amplitude. This was explained by the possible saturation of the NDVI signal, thereby rendering the NDVI seasonal amplitude less sensitive to detection of changes in dryland areas of the Sahel. This is supported by the results presented here (Fig. 4C and Fig. 5) showing that the saturation effect has an impact on biomass estimation for the greener parts of the Sahelian drylands.

5.4. Potentials of the VOD dataset

Vegetation long-term trend analysis based on different AHVRR NDVI products have been performed from regional to global scales to assist discussions on land degradation trends in drylands in general and in the Sahel in particular (Fensholt et al., 2012; Herrmann, Sall, & Sy, 2014; Mbow, Brandt, Ouedraogo, de Leeuw, & Marshall, 2015; Olsson et al., 2005; Prince, Wessels, Tucker, & Nicholson, 2007). The quality of these NDVI products and derived greening/browning trends have been scrutinized due to challenges in producing consistent time series from multiple sensor systems (Beck et al., 2011; de Beurs & Henebry, 2004; Tian et al., 2015). The long-term VOD dataset derived from passive microwave observations provides an important independent source to the NDVI based approaches for land degradation assessment and the results presented here are likely to facilitate the future interpretation of vegetation trend analysis based on VOD data. Moreover, estimations of woody cover in global drylands are likely to benefit from the unique capabilities of VOD data as shown here. Specifically, there is a long-standing debate on the development of the woody cover of the Sahel. Available studies of woody cover change are limited to local scales, covering different periods and thus providing contradictory results that are not directly comparable: While some studies have reported decreases in woody cover (and thus presumably also in biomass) (Gonzalez, Tucker, & Sy, 2012) others have provided evidence

for increases in woody cover (or related variables) (Brandt et al., 2015; Hiernaux et al., 2009; Spiekermann, Brandt, & Samimi, 2015). By calibration with existing static woody cover maps (e.g. Brandt et al. (2016)), the VOD dataset could potentially provide a spatio-temporally continuous estimation of woody cover changes in the Sahel since early 1990s. The coarse spatial resolution of VOD impedes its applicability at the local scale, but is of less concern for studies at regional, continental or global scales.

6. Conclusion and outlook

An improved understanding of the characteristics and responses of VOD to vegetation variations is achieved by comparison with the well-studied GIMMS3g AVHRR NDVI and *in situ* measurements in the semi-arid Senegalese Sahel, covering a gradient of mixtures of herbaceous and woody vegetation in drylands. VOD has proven to be an efficient proxy for green biomass of the entire vegetation stratum (both herbaceous and woody plant foliage). VOD shows an increased sensitivity to information on the woody plant foliage and is also found to be less affected by saturation effect as compared to NDVI in the greener parts of dryland areas. The different sensitivity of VOD and NDVI to total water content and chlorophyll abundance respectively is found to cause different seasonal metrics to be optimal for biomass monitoring amongst the two sensor systems. The integration of the greenness seasonality (NDVI small integral) is most closely related to *in situ* measured biomass, while the VOD works equally well as a proxy for biomass when used as a "snapshot" in time (October, when the *in situ green* biomass was measured). Also, the annual sum of VOD was found to perform well due to possible linkage between water content in the persistent part of the woody plants during dry season and foliage production during the growing season.

VOD appears to be less sensitive to vegetation species composition in monitoring dryland biomass production as compared to greenness measures derived from visible/near-infrared parts of the spectrum. Yet, further strong evidence is needed to support this conclusion. VOD is a promising proxy for the total biomass (both green and woody biomass) as it is also sensitive to the water content in the standing wood mass. However, the different relationships of water content to green and woody biomass need to be corrected for. A complementary use of VOD and NDVI would allow for more complete monitoring of dryland vegetation resources. With the higher sensitivity of VOD to woody vegetation water content, the long-term VOD dataset will help to improve our understanding of woody cover/biomass variations in drylands which is currently a challenge for regional/large scale optical remote sensing. On the other hand seasonal metrics of NDVI are still well suited for monitoring of green vegetation and obviously the capabilities of doing so with high spatial resolution is of importance for many applications. Except for the VOD, there are several other passive microwave-based vegetation indices, such as the microwave polarization difference index (MPDI) (Becker & Choudhury, 1988), the microwave emissivity difference vegetation index (EDVI) (Min & Lin, 2006) and the microwave vegetation indices (MVIs) (Shi et al., 2008). An inter-comparison between them would be of benefit for potential users.

Appendix A. Supplementary data

Supplementary data to this article can be found online at http://dx.doi.org/10.1016/j.rse.2016.02.056.

References

Achard, F., & Blasco, F. (1990). Analysis of vegetation seasonal evolution and mapping of forest cover in West Africa with the use of NOAA AVHRR HRPT data. *Photogrammetric Engineering & Remote Sensing, 56*, 1359–1365.

Adeel, Z., Safriel, U., Niemeijer, D., White, R., de Kalbermatten, G., Glantz, M., ... Yapi-Gnaore, V. (2005). *Ecosystems and human well-being: Desertification synthesis. A report of the millennium ecosystem assessment.* Washington, DC: World Resources Institute.

Ahearn, S. C., & de Rooy, C. (1996). Monitoring the effects of Dracunculiasis remediation on agricultural productivity using satellite data. *International Journal of Remote Sensing, 17*, 917–929.

Ahlstrom, A., Raupach, M. R., Schurgers, G., Smith, B., Arneth, A., Jung, M., ... Zeng, N. (2015). The dominant role of semi-arid ecosystems in the trend and variability of the land CO$_2$ sink. *Science, 348*, 895–899.

Andela, N., Liu, Y. Y., van Dijk, A. I. J. M., de Jeu, R. A. M., & McVicar, T. R. (2013). Global changes in dryland vegetation dynamics (1988–2008) assessed by satellite remote sensing: Comparing a new passive microwave vegetation density record with reflective greenness data. *Biogeosciences, 10*, 6657–6676.

Beck, H. E., McVicar, T. R., van Dijk, A. I. J. M., Schellekens, J., de Jeu, R. A. M., & Bruijnzeel, L. A. (2011). Global evaluation of four AVHRR–NDVI data sets: Intercomparison and assessment against Landsat imagery. *Remote Sensing of Environment, 115*, 2547–2563.

Becker, F., & Choudhury, B. J. (1988). Relative sensitivity of normalized difference vegetation index (NDVI) and microwave polarization difference index (MPDI) for vegetation and desertification monitoring. *Remote Sensing of Environment, 24*, 297–311.

Brandt, M., Hiernaux, P., Tagesson, T., Verger, A., Rasmussen, K., Diouf, A. A., ... Fensholt, R. (2016). Woody plant cover estimation in drylands from earth observation based seasonal metrics. *Remote Sensing of Environment, 172*, 28–38.

Brandt, M., Mbow, C., Diouf, A. A., Verger, A., Samimi, C., & Fensholt, R. (2015). Ground- and satellite-based evidence of the biophysical mechanisms behind the greening Sahel. *Global Change Biology, 1610-1620*.

Cao, C., Xiong, X., Wu, A., & Wu, X. (2008). Assessing the consistency of AVHRR and MODIS L1B reflectance for generating fundamental climate data records. *Journal of Geophysical Research-Atmospheres, 113*.

Choudhury, B. J., Tucker, C. J., Golus, R. E., & Newcomb, W. W. (1987). Monitoring vegetation using Nimbus-7 scanning multichannel microwave radiometer's data. *International Journal of Remote Sensing, 8*, 533–538.

Cissé, M. I. (1980). The browse production of some trees of the Sahel: Relationships between maximum foliage biomass and various physical parameters. *Browse in Africa* (pp. 205–210). Ethiopia: ILCA Addis Ababa.

Cui, Q., Shi, J., Du, J., Zhao, T., & Xiong, C. (2015). An approach for monitoring global vegetation based on multiangular observations from SMOS. *Selected Topics in Applied Earth Observations and Remote Sensing, IEEE Journal of, 8*, 604–616.

Dardel, C., Kergoat, L., Hiernaux, P., Mougin, E., Grippa, M., & Tucker, C. J. (2014). Re-greening Sahel: 30 years of remote sensing data and field observations (Mali, Niger). *Remote Sensing of Environment, 140*, 350–364.

de Beurs, K. M., & Henebry, G. M. (2004). Trend analysis of the pathfinder AVHRR land (PAL) NDVI data for the deserts of central Asia. *IEEE Geoscience and Remote Sensing Letters, 1*, 282–286.

de Jong, R., de Bruin, S., de Wit, A., Schaepman, M. E., & Dent, D. L. (2011). Analysis of monotonic greening and browning trends from global NDVI time-series. *Remote Sensing of Environment, 115*, 692–702.

Diallo, O., Diouf, A., Hanan, N. P., Ndiaye, A., & PRÉVost, Y. (1991). AVHRR monitoring of savanna primary production in Senegal, West Africa: 1987–1988. *International Journal of Remote Sensing, 12*, 1259–1279.

Diouf, A., & Lambin, E. F. (2001). Monitoring land-cover changes in semi-arid regions: Remote sensing data and field observations in the Ferlo, Senegal. *Journal of Arid Environments, 48*, 129–148.

Diouf, A., Brandt, M., Verger, A., Jarroudi, M., Djaby, B., Fensholt, R., ... Tychon, B. (2015). Fodder biomass monitoring in sahelian rangelands using phenological metrics from FAPAR time series. *Remote Sensing, 7*, 9122.

Diouf, A., Sall, M., Wélé, A., & Dramé, M. (1998). Sampling method of primary production in the field (technical document). In (p. 9): Centre de Suivi Ecologique of Dakar

Evans, J., & Geerken, R. (2004). Discrimination between climate and human-induced dryland degradation. *Journal of Arid Environments, 57*, 535–554.

Fensholt, R. (2004). Earth observation of vegetation status in the Sahelian and Sudanian West Africa: Comparison of terra MODIS and NOAA AVHRR satellite data. *International Journal of Remote Sensing, 25*, 1641–1659.

Fensholt, R., & Proud, S. R. (2012). Evaluation of earth observation based global long term vegetation trends — Comparing GIMMS and MODIS global NDVI time series. *Remote Sensing of Environment, 119*, 131–147.

Fensholt, R., Anyamba, A., Huber, S., Proud, S. R., Tucker, C. J., Small, J., ... Shisanya, C. (2011). Analysing the advantages of high temporal resolution geostationary MSG SEVIRI data compared to Polar Operational Environmental Satellite data for land

surface monitoring in Africa. *International Journal of Applied Earth Observation and Geoinformation*, 13, 721–729.

Fensholt, R., Anyamba, A., Stisen, S., Sandholt, I., Pak, E., & Small, J. (2007). Comparisons of compositing period length for vegetation index data from polar-orbiting and geostationary satellites for the cloud-prone region of West Africa. *Photogrammetric Engineering & Remote Sensing*, 73, 297–309.

Fensholt, R., Horion, S., Tagesson, T., Ehammer, A., Ivits, E., & Rasmussen, K. (2015). Global-scale mapping of changes in ecosystem functioning from earth observation-based trends in total and recurrent vegetation. *Global Ecology and Biogeography*, 24, 1003–1017.

Fensholt, R., Langanke, T., Rasmussen, K., Reenberg, A., Prince, S. D., Tucker, C., ... Wessels, K. (2012). Greenness in semi-arid areas across the globe 1981–2007 — An earth observing satellite based analysis of trends and drivers. *Remote Sensing of Environment*, 121, 144–158.

Fensholt, R., Rasmussen, K., Kaspersen, P., Huber, S., Horion, S., & Swinnen, E. (2013). Assessing land degradation/recovery in the African Sahel from long-term earth observation based primary productivity and precipitation relationships. *Remote Sensing*, 5, 664–686.

Fensholt, R., Rasmussen, K., Nielsen, T. T., & Mbow, C. (2009). Evaluation of earth observation based long term vegetation trends — Intercomparing NDVI time series trend analysis consistency of Sahel from AVHRR GIMMS, Terra MODIS and SPOT VGT data. *Remote Sensing of Environment*, 113, 1886–1898.

Fuller, D. O. (1998). Trends in NDVI time series and their relation to rangeland and crop production in Senegal, 1987–1993. *International Journal of Remote Sensing*, 19, 2013–2018.

Gitelson, A. A., Kaufman, Y. J., & Merzlyak, M. N. (1996). Use of a green channel in remote sensing of global vegetation from EOS-MODIS. *Remote Sensing of Environment*, 58, 289–298.

Goetz, S. J., Prince, S. D., Goward, S. N., Thawley, M. M., & Small, J. (1999). Satellite remote sensing of primary production: an improved production efficiency modeling approach. *Ecological Modelling*, 122, 239–255.

Gonzalez, P., Tucker, C. J., & Sy, H. (2012). Tree density and species decline in the African Sahel attributable to climate. *Journal of Arid Environments*, 78, 55–64.

Gruhier, C., de Rosnay, P., Hasenauer, S., Holmes, T., de Jeu, R., Kerr, Y., ... Zribi, M. (2010). Soil moisture active and passive microwave products: intercomparison and evaluation over a Sahelian site. *Hydrology and Earth System Sciences*, 14, 141–156.

Guan, K., Wood, E. F., Medvigy, D., Kimball, J., Pan, M., Caylor, K. K., ... Jones, M. O. (2014). Terrestrial hydrological controls on land surface phenology of African savannas and woodlands. *Journal of Geophysical Research: Biogeosciences*, 119 2013JG002572.

Herrmann, S. M., Sall, I., & Sy, O. (2014). People and pixels in the Sahel: A study linking coarse-resolution remote sensing observations to land users' perceptions of their changing environment in Senegal. *Ecology and Society*, 19.

Hiernaux, P. (1980). Inventory of the browse potential of bushes, trees and shrubs in an area of the Sahel in Mali: Method and initial results. *Browse in Africa*, 205.

Hiernaux, P., Diarra, L., Trichon, V., Mougin, E., Soumaguel, N., & Baup, F. (2009). Woody plant population dynamics in response to climate changes from 1984 to 2006 in Sahel (Gourma, Mali). *Journal of Hydrology S0022-1694(09)00135-8*, HYDROL 16508.

Holben, B. N. (1986). Characteristics of maximum-value composite images from temporal AVHRR data. *International Journal of Remote Sensing*, 7, 1417–1434.

Horion, S., Fensholt, R., Tagesson, T., & Ehammer, A. (2014). Using earth observation-based dry season NDVI trends for assessment of changes in tree cover in the Sahel. *International Journal of Remote Sensing*, 35, 2493–2515.

Huber, S., Fensholt, R., & Rasmussen, K. (2011). Water availability as the driver of vegetation dynamics in the African Sahel from 1982 to 2007. *Global and Planetary Change*, 76, 186–195.

Huete, A. R. (1988). A soil-adjusted vegetation index (SAVI). *Remote Sensing of Environment*, 25, 295–309.

Jackson, T. J., & Schmugge, T. J. (1991). Vegetation effects on the microwave emission of soils. *Remote Sensing of Environment*, 36, 203–212.

Jackson, T. J., Cosh, M. H., Bindlish, R., Starks, P. J., Bosch, D. D., Seyfried, M., ... Jinyang, D. (2010). Validation of advanced microwave scanning radiometer soil moisture products. *IEEE Transactions on Geoscience and Remote Sensing*, 48, 4256–4272.

Jeyaseelan, A. T., Roy, P. S., & Young, S. S. (2007). Persistent changes in NDVI between 1982 and 2003 over India using AVHRR GIMMS (global inventory modeling and mapping studies) data. *International Journal of Remote Sensing*, 28, 4927–4946.

Jones, M. O., Jones, L. A., Kimball, J. S., & McDonald, K. C. (2011). Satellite passive microwave remote sensing for monitoring global land surface phenology. *Remote Sensing of Environment*, 115, 1102–1114.

Jones, M. O., Kimball, J. S., & Jones, L. A. (2013). Satellite microwave detection of boreal forest recovery from the extreme 2004 wildfires in Alaska and Canada. *Global Change Biology*, 19, 3111–3122.

Jones, M. O., Kimball, J. S., Jones, L. A., & McDonald, K. C. (2012). Satellite passive microwave detection of North America start of season. *Remote Sensing of Environment*, 123, 324–333.

Jones, M. O., Kimball, J. S., & Nemani, R. R. (2014). Asynchronous Amazon forest canopy phenology indicates adaptation to both water and light availability. *Environmental Research Letters*, 9.

Jonsson, P., & Eklundh, L. (2002). Seasonality extraction by function fitting to time-series of satellite sensor data. *IEEE Transactions on Geoscience and Remote Sensing*, 40, 1824–1832.

Jonsson, P., & Eklundh, L. (2004). TIMESAT — A program for analyzing time-series of satellite sensor data. *Computers & Geosciences*, 30, 833–845.

Konings, A. G., Piles, M., Rötzer, K., McColl, K. A., Chan, S. K., & Entekhabi, D. (2016). Vegetation optical depth and scattering albedo retrieval using time series of dual-polarized L-band radiometer observations. *Remote Sensing of Environment*, 172, 178–189.

Le Houérou, H. N. (1980). The rangelands of the Sahel. *Journal of Range Management*, 33, 41–46.

Leroux, D. J., Kerr, Y. H., Al Bitar, A., Bindlish, R., Jackson, T. J., Berthelot, B., & Portet, G. (2014). Comparison between SMOS, VUA, ASCAT, and ECMWF soil moisture products over four watersheds in U.S. *Geoscience and Remote Sensing, IEEE Transactions on*, 52, 1562–1571.

Liu, Y. Y., de Jeu, R. A. M., McCabe, M. F., Evans, J. P., & van Dijk, A. I. J. M. (2011a). Global long-term passive microwave satellite-based retrievals of vegetation optical depth. *Geophysical Research Letters*, 38.

Liu, Y. Y., Dorigo, W. A., Parinussa, R. M., de Jeu, R. A. M., Wagner, W., McCabe, M. F., ... van Dijk, A. I. J. M. (2012). Trend-preserving blending of passive and active microwave soil moisture retrievals. *Remote Sensing of Environment*, 123, 280–297.

Liu, Y. Y., Evans, J. P., McCabe, M. F., de Jeu, R. A. M., van Dijk, A. I. J. M., Dolman, A. J., & Saizen, I. (2013a). Changing climate and overgrazing are decimating Mongolian steppes. *PloS One*, 8, e57599.

Liu, Y. Y., Parinussa, R. M., Dorigo, W. A., De Jeu, R. A. M., Wagner, W., van Dijk, A. I. J. M., ... Evans, J. P. (2011b). Developing an improved soil moisture dataset by blending passive and active microwave satellite-based retrievals. *Hydrology and Earth System Sciences*, 15, 425–436.

Liu, Y. Y., van Dijk, A. I. J. M., de Jeu, R. A. M., Canadell, J. G., McCabe, M. F., Evans, J. P., & Wang, G. (2015). Recent reversal in loss of global terrestrial biomass. *Nature Climate Change*, 5, 470–474.

Liu, Y. Y., van Dijk, A. I. J. M., McCabe, M. F., Evans, J. P., & de Jeu, R. A. M. (2013b). Global vegetation biomass change (1988–2008) and attribution to environmental and human drivers. *Global Ecology and Biogeography*, 22, 692–705.

Los, S. O. (1998). Estimation of the ratio of sensor degradation between NOAA AVHRR channels 1 and 2 from monthly NDVI composites. *IEEE Transactions on Geoscience and Remote Sensing*, 36, 206–213.

Mbow, C., Brandt, M., Ouedraogo, I., de Leeuw, J., & Marshall, M. (2015). What four decades of earth observation tell us about land degradation in the Sahel? *Remote Sensing*, 7, 4048.

Mbow, C., Fensholt, R., Rasmussen, K., & Diop, D. (2013). Can vegetation productivity be derived from greenness in a semi-arid environment? Evidence from ground-based measurements. *Journal of Arid Environments*, 97, 56–65.

Meesters, A. G. C. A., de Jeu, R. A. M., & Owe, M. (2005). Analytical derivation of the vegetation optical depth from the microwave polarization difference index. *IEEE Geoscience and Remote Sensing Letters*, 2, 121–123.

Meroni, M., Rembold, F., Verstraete, M., Gommes, R., Schucknecht, A., & Beye, G. (2014). Investigating the relationship between the inter-annual variability of satellite-derived vegetation phenology and a proxy of biomass production in the Sahel. *Remote Sensing*, 6, 5868.

Milich, L., & Weiss, E. (2000). GAC NDVI images: relationship to rainfall and potential evaporation in the grazing lands of The Gourma (northern Sahel) and in the croplands of the Niger-Nigeria border (southern Sahel). *International Journal of Remote Sensing*, 21, 261–280.

Min, Q., & Lin, B. (2006). Remote sensing of evapotranspiration and carbon uptake at Harvard Forest. *Remote Sensing of Environment*, 100, 379–387.

Mo, T., Choudhury, B. J., Schmugge, T. J., Wang, J. R., & Jackson, T. J. (1982). A model for microwave emission from vegetation-covered fields. *Journal of Geophysical Research: Oceans*, 87, 11229–11237.

Mougin, E., Demarez, V., Diawara, M., Hiernaux, P., Soumaguel, N., & Berg, A. (2014). Estimation of LAI, fAPAR and fCover of Sahel rangelands (Gourma, Mali). *Agricultural and Forest Meteorology*, 198–199, 155–167.

Mougin, E., Lo Seena, D., Rambal, S., Gaston, A., & Hiernaux, P. (1995). A regional Sahelian grassland model to be coupled with multispectral satellite data. I: Model description and validation. *Remote Sensing of Environment*, 52, 181–193.

Myneni, R. B., & Hall, F. G. (1995). The interpretation of spectral vegetation indexes. *IEEE Transactions on Geoscience and Remote Sensing*, 33, 481–486.

Myneni, R. B., Keeling, C. D., Tucker, C. J., Asrar, G., & Nemani, R. R. (1997). Increased plant growth in the northern high latitudes from 1981 to 1991. *Nature*, 386, 698–702.

Nemani, R. R., Keeling, C. D., Hashimoto, H., Jolly, W. M., Piper, S. C., Tucker, C. J., ... Running, S. W. (2003). Climate-driven increases in global terrestrial net primary production from 1982 to 1999. *Science*, 300, 1560–1563.

Njoku, E. G., & Chan, S. K. (2006). Vegetation and surface roughness effects on AMSR-E land observations. *Remote Sensing of Environment*, 100, 190–199.

Novella, N. S., & Thiaw, W. M. (2013). African rainfall climatology version 2 for famine early warning systems. *Journal of Applied Meteorology and Climatology*, 52, 588–606.

Olsen, J. L., Miehe, S., Ceccato, P., & Fensholt, R. (2015). Does EO NDVI seasonal metrics capture variations in species composition and biomass due to grazing in semi-arid grassland savannas? *Biogeosciences*, 12, 4407–4419.

Olsson, L., Eklundh, L., & Ardö, J. (2005). A recent greening of the Sahel — Trends, patterns and potential causes. *Journal of Arid Environments*, 63, 556–566.

Owe, M., de Jeu, R., & Holmes, T. (2008). Multisensor historical climatology of satellite-derived global land surface moisture. *Journal of Geophysical Research-Earth Surface*, 113.

Owe, M., de Jeu, R., & Walker, J. (2001). A methodology for surface soil moisture and vegetation optical depth retrieval using the microwave polarization difference index. *IEEE Transactions on Geoscience and Remote Sensing*, 39, 1643–1654.

Pinzon, J., & Tucker, C. (2014). A non-stationary 1981–2012 AVHRR NDVI3$_g$ time series. *Remote Sensing*, 6, 6929–6960.

Pinzon, J., Brown, M. E., & Tucker, C. J. (2005). Satellite time series correction of orbital drift artifacts using empirical mode decomposition. In N. Huang (Ed.), *Hilbert-Huang transform: Introduction and applications* (pp. 167–186).

Poulter, B., Frank, D., Ciais, P., Myneni, R. B., Andela, N., Bi, J., ... van der Werf, G. R. (2014). Contribution of semi-arid ecosystems to interannual variability of the global carbon cycle. *Nature*, 509, 600–603.

Prince, S. D. (1991). Satellite remote sensing of primary production: comparison of results for Sahelian grasslands 1981–1988. *International Journal of Remote Sensing, 12*, 1301–1311.

Prince, S. D., & Goward, S. N. (1995). Global primary production: A remote sensing approach. *Journal of Biogeography, 22*, 815–835.

Prince, S. D., Wessels, K. J., Tucker, C. J., & Nicholson, S. E. (2007). Desertification in the Sahel: A reinterpretation of a reinterpretation. *Global Change Biology, 13*, 1308–1313.

Sellers, P. J. (1985). Canopy reflectance, photosynthesis and transpiration. *International Journal of Remote Sensing, 6*, 1335–1372.

Shi, J., Jackson, T., Tao, J., Du, J., Bindlish, R., Lu, L., & Chen, K. S. (2008). Microwave vegetation indices for short vegetation covers from satellite passive microwave sensor AMSR-E. *Remote Sensing of Environment, 112*, 4285–4300.

Spiekermann, R., Brandt, M., & Samimi, C. (2015). Woody vegetation and land cover changes in the Sahel of Mali (1967–2011). *International Journal of Applied Earth Observation and Geoinformation, 34*, 113–121.

Tagesson, T., Mastepanov, M., Molder, M., Tamstorf, M. P., Eklundh, L., Smith, B., ... Strom, L. (2013). Modelling of growing season methane fluxes in a high-Arctic wet tundra ecosystem 1997–2010 using in situ and high-resolution satellite data. *Tellus Series B-Chemical and Physical Meteorology, 65*.

Tian, F., Fensholt, R., Verbesselt, J., Grogan, K., Horion, S., & Wang, Y. (2015). Evaluating temporal consistency of long-term global NDVI datasets for trend analysis. *Remote Sensing of Environment, 163*, 326–340.

Tian, F., Wang, Y., Fensholt, R., Wang, K., Zhang, L., & Huang, Y. (2013). Mapping and evaluation of NDVI trends from synthetic time series obtained by blending Landsat and MODIS data around a coalfield on the loess plateau. *Remote Sensing, 5*, 4255–4279.

Tucker, C. J. (1979). Red and photographic infrared linear combinations for monitoring vegetation. *Remote Sensing of Environment, 8*, 127–150.

Tucker, C. J., & Sellers, P. J. (1986). Satellite remote sensing of primary production. *International Journal of Remote Sensing, 7*, 1395–1416.

Tucker, C. J., Pinzon, J. E., Brown, M. E., Slayback, D. A., Pak, E. W., Mahoney, R., ... El Saleous, N. (2005). An extended AVHRR 8-km NDVI dataset compatible with MODIS and SPOT vegetation NDVI data. *International Journal of Remote Sensing, 26*, 4485–4498.

Tucker, C. J., Vanpraet, C., Boerwinkel, E., & Gaston, A. (1983). Satellite remote sensing of total dry matter production in the Senegalese Sahel. *Remote Sensing of Environment, 13*, 461–474.

Vermote, E., & Kaufman, Y. J. (1995). Absolute calibration of AVHRR visible and near-infrared channels using ocean and cloud views. *International Journal of Remote Sensing, 16*, 2317–2340.

Wessels, K. J., Prince, S. D., Zambatis, N., MacFadyen, S., Frost, P. E., & Van Zyl, D. (2006). Relationship between herbaceous biomass and 1-km^2 advanced very high resolution radiometer (AVHRR) NDVI in Kruger National Park, South Africa. *International Journal of Remote Sensing, 27*, 951–973.

Wigneron, J. -P., Chanzy, A., Calvet, J. -C., & Bruguier, N. (1995). A simple algorithm to retrieve soil moisture and vegetation biomass using passive microwave measurements over crop fields. *Remote Sensing of Environment, 51*, 331–341.

Wu, X. Q., Sullivan, J. T., & Heidinger, A. K. (2010). Operational calibration of the Advanced Very High Resolution Radiometer (AVHRR) visible and near-infrared channels. *Canadian Journal of Remote Sensing, 36*, 602–616.

Zeng, J., Li, Z., Chen, Q., Bi, H., Qiu, J., & Zou, P. (2015). Evaluation of remotely sensed and reanalysis soil moisture products over the Tibetan Plateau using in-situ observations. *Remote Sensing of Environment, 163*, 91–110.